Atmos. Chem. Phys., 17, 1641–1651, 2017
www.atmos-chem-phys.net/17/1641/2017/
doi:10.5194/acp-17-1641-2017

Atmospheric Chemistry and Physics
Open Access
EGU

Understanding severe winter haze events in the North China Plain in 2014: roles of climate anomalies

Zhicong Yin[1,2], **Huijun Wang**[1,2,3], **and Huopo Chen**[2,3,1]

[1]Key Laboratory of Meteorological Disaster, Ministry of Education/Joint International Research Laboratory of Climate and Environment Change (ILCEC)/Collaborative Innovation Center on Forecast and Evaluation of Meteorological Disasters (CIC-FEMD), Nanjing University of Information Science & Technology, Nanjing 210044, China
[2]Nansen-Zhu International Research Centre, Institute of Atmospheric Physics, Chinese Academy of Sciences, Beijing, China
[3]Climate Change Research Center, Chinese Academy of Sciences, Beijing, China

Correspondence to: Zhicong Yin (yinzhc@163.com)

Received: 18 July 2016 – Published in Atmos. Chem. Phys. Discuss.: 1 August 2016
Revised: 15 November 2016 – Accepted: 27 December 2016 – Published: 2 February 2017

Abstract. Atmospheric pollution has become a serious environmental and social problem in China. Over the past 30 years, the number of winter (December–February) haze days over the North China Plain (WHD_{NCP}) was greatest in 2014. In addition to anthropogenic influence, climate anomalies also played a role. Thus, it is necessary to analyze the anomalous atmosphere circulations associated with haze pollution of this year in detail. Near the surface, the weaker East Asian winter monsoon pattern, causing southerly winds over the North China Plain, could aggravate the situation of haze. In the lower and middle troposphere, taking the anticyclone circulation over North China as an intermediate system, the positive phases of the eastern Atlantic/western Russia (EA/WR), the western Pacific (WP), and the Eurasia (EU) patterns led to a worse air pollution dispersion condition that contributed to a larger number of WHD_{NCP}. In 2014, these three patterns could be recognized from the wind anomalies in the lower troposphere. The preceding autumn (September–November) Arctic sea ice (ASI) anomalies over the eastern Hemisphere and the warmer winter surface over Eurasia might have induced or intensified the positive EA/WR pattern in 2014. These two external forcings, together with the pre-autumn sea surface temperature anomalies in the Pacific, might have also stimulated or enhanced the positive EU-like patterns. The anomalous surface temperature in autumn 2014 was efficient in intensifying anomalous circulations such as the positive phase of the WP pattern. The opposite case of minimum WHD_{NCP} in 2010 further supports the mechanism of how EA/WR and WP patterns and associated external factors altered the local climate conditions to impact the WHD_{NCP}.

1 Introduction

Related to booming economic development, atmospheric pollution has become a serious environmental and social problem in China (Ding and Liu, 2014; Wang and Chen, 2016). Particularly after the persistent heavy fog and haze events in January 2013, haze pollution has become more severe (Zhang et al., 2014; Zhao et al., 2014; Li et al., 2015) and has shown to have certain negative effects on human health (Yin et al., 2011; Chen et al., 2013). The North China Plain (NCP), a location with very high population density, is one of three haze-prone regions in China. The winter (December–February) haze pollution over the NCP (34–43° N, 114–120° E) in 2013 and 2014 was the most serious of these events in the past 30 years (Yin et al., 2015a). Therefore, the objective of this study is to examine the related climate conditions (e.g., atmospheric circulation anomalies and external forcings) that were responsible for the extreme haze events in 2014.

There is no doubt that the anthropogenic emissions were the fundamental cause of the long-term variation in haze days (Wang et al., 2013). However, the impact of meteorological conditions is highlighted and the climate conditions are also vital contributors to the interannual variation in haze (Yang et al., 2016; Zhang et al., 2016). For example, the joint effect

of fast increase in total energy consumption, rapid decline of Arctic sea ice extent, and reduced precipitation and surface winds intensified the haze pollution in central North China after 2000 (Wang and Chen, 2016). Early studies have shown that the East Asian winter monsoon (EAWM) had weakened after 1986, which led to an increase in winter haze days (WHDs) over the NCP (WHD_{NCP}) (Yin et al., 2015a, b; Li et al., 2015). The decline in the preceding autumn (September–November) Arctic sea ice (ASI) from 1979 to 2012 greatly intensified haze pollution in eastern China, the variance contribution of which was 45–67 % (H. J. Wang et al., 2015). Sea surface temperature (SST) over the subtropical western Pacific (SWP) showed significantly negative correlation with WHD_{NCP}. SWP SST weakened EAWM circulation, leading to a favorable environment for haze with a stable atmosphere and potential for hygroscopic growth (Yin and Wang, 2016a).

The local anticyclone anomaly around the NCP was the most prominent circulation related to WHD_{NCP} (Yin and Wang, 2016a; Chen and Wang, 2015) and was located near the convergence area of two continental Rossby waves, i.e., Eurasia (EU) and eastern Atlantic/western Russia (EA/WR) patterns. The EU pattern, as defined by Wallace and Gutzler (1981), originated from the high-latitude polar region. The EU positive phase showed negative centers over the polar region (70–80° N, 60–90° E) and the Japan Sea (35–45° N, 120–140° E), as well as a positive center over Mongolia and North China (45–55° N, 90–110° E), which accounted for the severe drought in 2014 (Wang and He, 2015). Another Eurasian teleconnection, known as the EA/WR pattern (Barnston and Livezey, 1987), was composed of negative centers over the central North Atlantic and to the north of the Caspian Sea, as well as positive centers over Europe and North China. The positive phase of these two continental Rossby wave trains might have led to significant warming over the northern portion of East Asia (Liu et al., 2014), indicating weaker cold air. Therefore, we speculated that external forcings such as the SST, ASI, and land surface temperature (T_s) might impact teleconnection patterns in the atmosphere and then the teleconnection patterns could alter the local climate anomalies to modulate the WHD_{NCP} remotely. Climate research on haze pollution in China is quite a new endeavor but is still sparse, especially with respect to investigation into the mechanism that causes extreme haze events. Thus, the roles of climate anomalies in the winter haze in 2014 over the NCP were investigated in this study and were expected to improve prediction skill for WHD_{NCP}.

The remainder of this paper is organized as follows. The data and methods are described in Sect. 2. The climatic reality of severe WHD_{NCP} in 2014 and associated atmospheric circulations are analyzed in Sect. 3. Section 4 describes investigation of the physical mechanism using the singular value decomposition (SVD) technique. Brief conclusions and selected discussions are presented in Sect. 5.

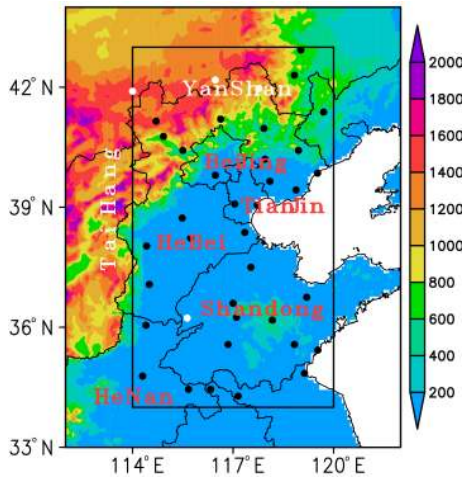

Figure 1. Topographic map (shading; unit: m) of North China and the locations of 39 NCP observation sites (urban: black circle; rural: white circle). The NCP area is represented by a black rectangle, and the names of provinces and mountains are written in red and white, respectively.

2 Datasets and methods

The China ground observations from 39 NCP stations (Fig. 1) collected by the National Meteorological Information Center of China from 1979 to 2015 were used to reconstruct the climatic WHD data (see Yin and Wang 2016a). Due to the quality and temporal range of the data, only four rural stations qualified for selection (white circles in Fig. 1). The routine meteorological measurements included relative humidity, visibility, and wind speed, which were collected four times per day, i.e., 02:00 local time (LT), 08:00 LT (00:00 UTC), 14:00 LT, and 20:00 LT. In this work, haze is recognized as when visibility falls below a certain threshold and the relative humidity is less than 90 %. After excluding other weather phenomena that affect visibility, we defined a haze day as a day with haze occurring at any of the four times. Most of the visibility observations have switched from manual to automatic since 1 January 2014, but the trial stations coded 54511, 54527, and 54623 were switched in 2013. Thus, the visibility threshold is 10 km before 1 January 2014 for most stations but before 1 December 2013 for the trial stations. After the switch, the threshold became 7.5 km, according to a report of the China Meteorology Administration (2014). To a certain extent, the WHD data of 2013 and 2014 are more qualitative than quantitative. To avoid continuity problems, the haze data for these 2 years were processed using composite analysis instead of correlation analysis in this study.

Haze is a multidisciplinary phenomenon that can be represented by visibility and humidity in meteorology, as well as by the concentration of the atmospheric composition in environmental science. In recent years, the atmospheric compo-

sitions involving the concentrations of SO_2, NO, NO_2, NO_x, CO, O_3, $PM_{2.5}$ (using a TEOM 1400a), and nephelometric turbidity (NEP) have been measured in Shangdianzi and Baolian (an urban site in Beijing; Zhao et al., 2011). The detailed atmospheric composition datasets were collected four times per day from 1 December 2014 to 28 February 2015. Hourly $PM_{2.5}$ data during 2004–2015 and 2008–2015 at Shangdianzi and Baolian Station, respectively, are used in this study. Shangdianzi Station, one of the six regional Global Atmosphere Watch (GAW) stations in China, is located at 40°39′ N, 117°7′ E, 293.3 m above sea level. As it is the only regional background GAW station in North China, the atmospheric composition at this location was chosen to best characterize the natural state or rather the background conditions of the atmosphere (Yao et al., 2012). The $PM_{2.5}$ data were monitored every 5 min using two methods: a tapered element oscillating microbalance (TEOM) and β-rays (since 2013).

In China, the temporal range and quality of the observed atmospheric compositions cannot support climatic haze research. To demonstrate whether the visibility-based reconstruction of haze data is representative, the hourly visibility and concentration of the atmospheric composition were shown, and the correlation coefficients were computed (Fig. S1 in the Supplement). In addition to significantly positive correlation with O_3, the correlation coefficients between visibility and seven compositions were all negative and exceeded the 99.99 % confidence level in winter 2014. $PM_{2.5}$ was the main reason for haze pollution, and the correlation coefficients with visibility in Beijing were −0.51 (Baolian) and −0.48 (Shangdianzi). When visibility was less than 7.5 and 1 km, the mean $PM_{2.5}$ mass concentrations at Baolian were approximately greater than 100 and 200 $\mu g\,m^{-3}$, respectively. Thus, the tendency and magnitude both showed that the derived haze datasets not only agreed with the meteorological standard but also satisfactorily represented the concentration of the atmospheric composition.

Monthly atmospheric data such as wind, geopotential height, temperature, and sea level pressure (SLP) are derived from the National Centers for Environmental Prediction/National Center for Atmospheric Research global reanalysis dataset with a horizontal resolution of 2.5° × 2.5° collected from 1979 to 2015 (Kalnay et al., 1996). The monthly mean planetary boundary layer height (PBLH, 1° × 1°) was derived from the ERA-Interim dataset (Dee et al., 2011). The monthly mean Extended Reconstructed Sea Surface Temperature (ERSST) datasets with a horizontal resolution of 2° × 2° collected from 1979 to 2015 were obtained from the National Oceanic and Atmospheric Administration (NOAA) (Smith et al., 2008). The ASI area was calculated using the ASI concentration data from the Hadley Centre's HadISST1 dataset with a resolution of 1° × 1° collected from 1979 to 2015 (Rayner et al., 2003). The EA/WR and WP indices were computed by the NOAA climate prediction center according to the rotated principal component analysis used by Barnston and Livezey (1987). The calculation procedure for the EU index was consistent with that of Wang and He (2015):

$$\begin{aligned}&\text{EU index} = \\ &\left[-1U\overline{H500}_{(70\text{–}80^\circ\text{ N},\,60\text{–}90^\circ\text{ E})} + 2\times\overline{H500}_{(45\text{–}55^\circ\text{ N},\,90\text{–}110^\circ\text{ E})}\right. \\ &\left.-1\times\overline{H500}_{(35\text{–}45^\circ\text{ N},\,120\text{–}140^\circ\text{ E})}\right]/4, \qquad (1)\end{aligned}$$

where $H500$ represents the geopotential height at 500 hPa and overbars denote the area average.

To verify the covariability between the atmosphere and external forcings (i.e., SST, ASI, and T_s), SVD and correlation analyses were applied after linear trends were removed. To some extent, the energy consumption varied continuously and linearly in eastern China and the socioeconomic components of WHD_{NCP} could be removed primitively by detrending, and then the interannual variability in haze pollution should be mainly the result of climatic anomalies. The anomalies in 2010, 2013, and 2014 were calculated relative to the climatic mean of 1979–2012. The site WHD data were converted into grids using the Cressman interpolation (Cressman, 1959), and WHD_{NCP} was computed as the mean value of the grid data.

3 Variations in WHD_{NCP} and associated atmospheric circulations

According to Fig. 2, WHD_{NCP} from 1979 to 2012 can be divided into two decadal stages, i.e., the first stage from 1979 to 1992 with an average of 45.1 days and the second decade from 1993 to 2012 with an average of 34.5 days. It is clear that WHD_{NCP} exhibited a rapid increase from winter 2010 onward with a large trend of 7.36 days yr^{-1}. The NCP is a haze-prone area in which WHD is distributed nonuniformly (Fig. 3a). Two regions exhibited greater WHD: the plain to the east of Taihang Mountains and to the south of Yan Mountains (PETSY) and the south of Shandong Province. As shown in Fig. 1, there were four rural stations, three of which were located near the Yan Mountains and corresponded to fewer WHDs. Another rural site near the boundaries of Shandong and Henan (BSH) showed fewer WHDs. Figure 3b shows the WHD anomalies in 2014 with respect to 1979–2012. In addition to a few sites, a larger number of WHDs occurred, especially on the BSH (rural area) and the northeast of Hebei. It is notable that WHDs in these two regions show significant increases, filling up the climatic WHD valley as shown in Fig. 3a. As a result, the haze-prone area joined together, indicating that the haze pollution was more serious in this region. Actually, the fast increase in WHDs in rural area was an obvious reflection of the severe haze disaster in recent years. At the same time, a larger number of WHDs occurred on PETSY and the south of Shandong Province. Recently, the haze pollution has become increasingly serious, as shown by the number of haze days and its coverage. The percentages of sites with greater than 30 and

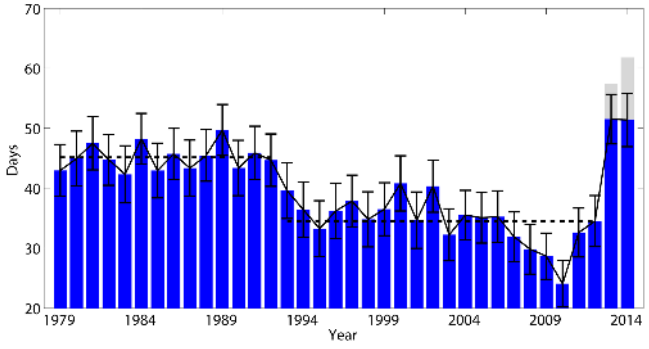

Figure 2. Variation in WHD_{NCP} from 1979 to 2014 (units: days); the error bar represents 1 standard error among the measured sites. For 2013–2014, the thresholds of 7.5 km (blue) and 10 km (gray) are both shown, and the dashed lines indicate the mean values for 1979–1992 and 1993–2012, respectively.

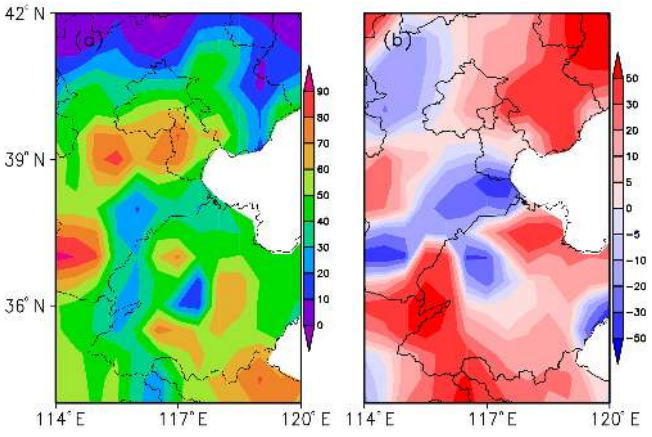

Figure 3. Distributions of WHD from 1979 to 2012 **(a)** and anomalies in 2014 relative to 1979–2012 **(b)**.

60 hazy days were 71.8 and 51.3 %, respectively, in 2014. As shown in Fig. S1, the mean $PM_{2.5}$ mass concentrations in Beijing were above 100 μg m^{-3} on hazy days, which indicated serious pollution in 2014. Although data continuity was influenced by the switch of the observation method in 2013, the observation that WHD_{NCP} in 2014 was greater than before showed robustness. Thus, it was reasonable to treat the year 2014 as a typical case for haze pollution over this region. As shown in Fig. 2, the NCP experienced the least WHDs in 2010, which could be analyzed as an inverse case of the extreme haze phenomena.

In the lower and middle layers of the troposphere, the correlation fields between WHD_{NCP} and $H500$ (UV850) represented obvious EA/WR and WP patterns (Fig. 4a–b). The EA/WR pattern originated from the north-central Atlantic and propagated through Europe, the north of the Caspian Sea and North China (Barnston and Livezey, 1987; Liu et al., 2014). The WP pattern showed two activity centers, i.e., the broad area of Southeast Asia and the northwestern Pacific

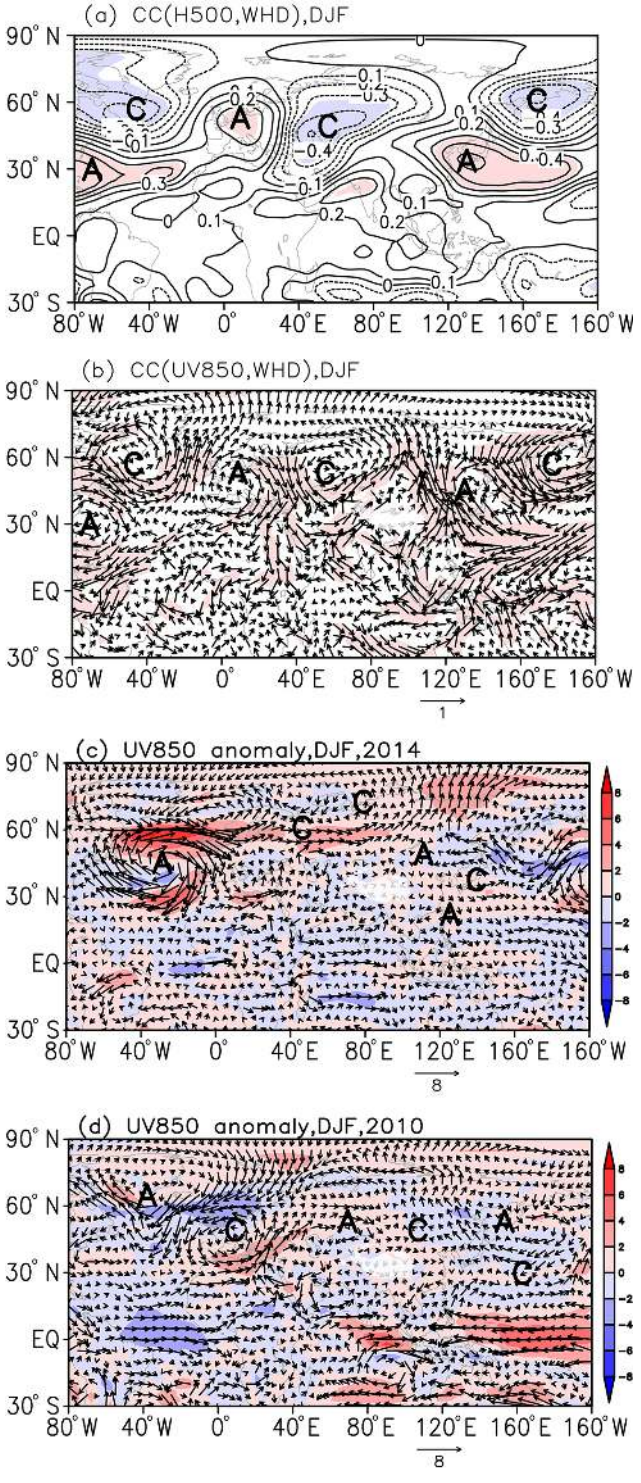

Figure 4. Correlation coefficients between WHD_{NCP} and winter $H500$ **(a)** / UV850 **(b)** from 1979 to 2012. The linear trend was removed, and shading indicates that the correlation coefficient exceeds the 95 % confidence level. UV850 (arrow) and speed (shading) anomalies in winter 2014 **(c)** and 2010 **(d)**. Letters A and C represent anticyclone and cyclone, respectively.

Table 1. Correlation coefficients between WHD_{NCP} and three teleconnection (EA/WR, WP, and EU) indices. A single asterisk (*) indicates that the result exceeded the 95 % confidence level, and double asterisks (**) indicate that it exceeded the 99 % confidence level. Note: OS means "original sequence", and "detrended" means that the linear trend was removed.

Pattern	OS	Detrended
EA/WR	0.36*	0.43**
WP	−0.06	0.41*
EU	0.34*	−0.13

and the Kamchatka Peninsula (Barnston and Livezey, 1987). In addition to EA/WR, the EU pattern was another continental Rossby wave train over Eurasia, which significantly impacted the climate of East Asia (Liu et al., 2014). Although the EU pattern was unclear in Fig. 4a–b, it can be recognized distinctively from the anomalous circulations in 2014 (Fig. 4c). The correlation coefficients between WHD_{NCP} and these three pattern indices were calculated (Table 1). After detrending, WHD_{NCP} showed significant positive correlation with both the EA/WR and WP patterns, indicating the remote impact on WHD_{NCP} from land and sea. The correlation between EU and WHD_{NCP} was initially significantly positive but became insignificant after detrending. Considering that EU could be recognized from low, middle, and high layers in winter 2014, the EU pattern was still treated as a possible circulation correlated with WHD_{NCP}. These teleconnection patterns might contribute to WHD_{NCP} by impacting the pivotal and local anticyclone anomalies (i.e., the local climate conditions) over the NCP (Fig. 4a–b). The deep and broad positive anomalies resulted in a thinner boundary layer by suppressing vertical movement and progressed easterly to weaken the East Asia Jet Stream (EAJS), indicating weaker meridional cold air. Near the surface, the negative SLP anomalies in the Siberia region and the Chinese mainland and the positive SLP anomalies over the western Pacific led to a reduced pressure gradient and weakened EAWM (Fig. 5a). The weaker EAWM induced the southeasterly anomalies and reduced the surface wind speed (Fig. 5b), indicating weaker cold air and warmer land surface over the NCP (Fig. 5a). Influenced by the circulations with weaker cold air, horizontal dispersion of the atmospheric particulates was impeded. Near the NCP, the anomalous anticyclone also existed, indicating weaker vertical motion. The main physical process was that the climate teleconnection patterns altered the local climate conditions, and then influenced the dispersion capacity of the local atmosphere. That is, when the positive pattern of EA/WR, WP, and EU occurred together or separately, the anomalous anticyclone over the NCP and Japan Sea was enhanced from the surface to the middle troposphere; thus, the convection or vertical motion was confined. The southerly anomalies on the left side of this anticyclone weakened the cold air and wind speed, but brought about humid flow. Under such local climate anomalies, the vertical dispersion and horizontal dispersion of atmospheric particulates were both restricted, and thus the pollutant gathered in a narrow space and resulted in the occurrence of haze.

In winter 2014, many extreme climatic events occurred, such as severe drought and high temperatures in the NCP (H. J. Wang et al., 2015). Corresponding external forcings should be observed as the background of these extreme synoptic and climatic events, which might have persistently impacted the winter atmospheric circulations and led to an irregular distribution of teleconnection patterns in winter. It should be noted that EA/WR pattern in winter 2014 was distributed slightly westwards and broadly. Nevertheless, the three eastern centers of EA/WR, WP, and EU patterns could be recognized (Fig. 4c). The linkage anticyclone of these three teleconnection patterns was enhanced and modulated the local climate conditions. The NCP area was influenced by the anomalous high resulting in lower PBLH (Fig. 6). The southerly at the high latitudes deadened the cold air from its main source and enhanced accumulation of local air pollutants, so the atmospheric matters gathered easily. Near the surface, the negative SLP anomalies occupied the whole Asian continent and Japan Sea, which weakened the continental cold high and stimulated significant southerly anomalies to the north of 50° N with the weaker Aleutian low. The weaker EAWM circulations near the surface blocked the cold air from high latitudes and resulted in a warmer surface (D. Q. Wang et al., 2015). There were positive SLP anomalies over the South China Sea and East China Sea that induced southerly and smaller surface wind speed over the coastal area in the east of China (Fig. 5c–d). The dispersion of atmosphere over the NCP was limited, so the high pollutant emissions were concentrated in a narrow space and severe haze events occurred easily. Large-scale circulations, such as the negative phase of EA/WR and WP, were quite clear in 2010 (Fig. 4d). Near the surface, the anomalous circulations were distributed similarly but almost opposite, i.e., the stronger continental cold high and oceanic low (Fig. 5e), the northerly and stronger surface wind over the NCP (Fig. 5f), and the higher PBLH (Fig. 6). The atmospheric dispersion capacity was heightened by the stronger cold air and vertical movement. This observation further supports the speculation that the anomalous EA/WR and WP patterns contributed to significant changes in WHD_{NCP} by altering the local climate conditions. The anomalies of the EU pattern in winter 2010 were not as significant as those in 2014. As shown by Table 1, the relationship between WHD_{NCP} and the EU index weakened after detrending, illustrating that the correlation was much weaker than the other two patterns.

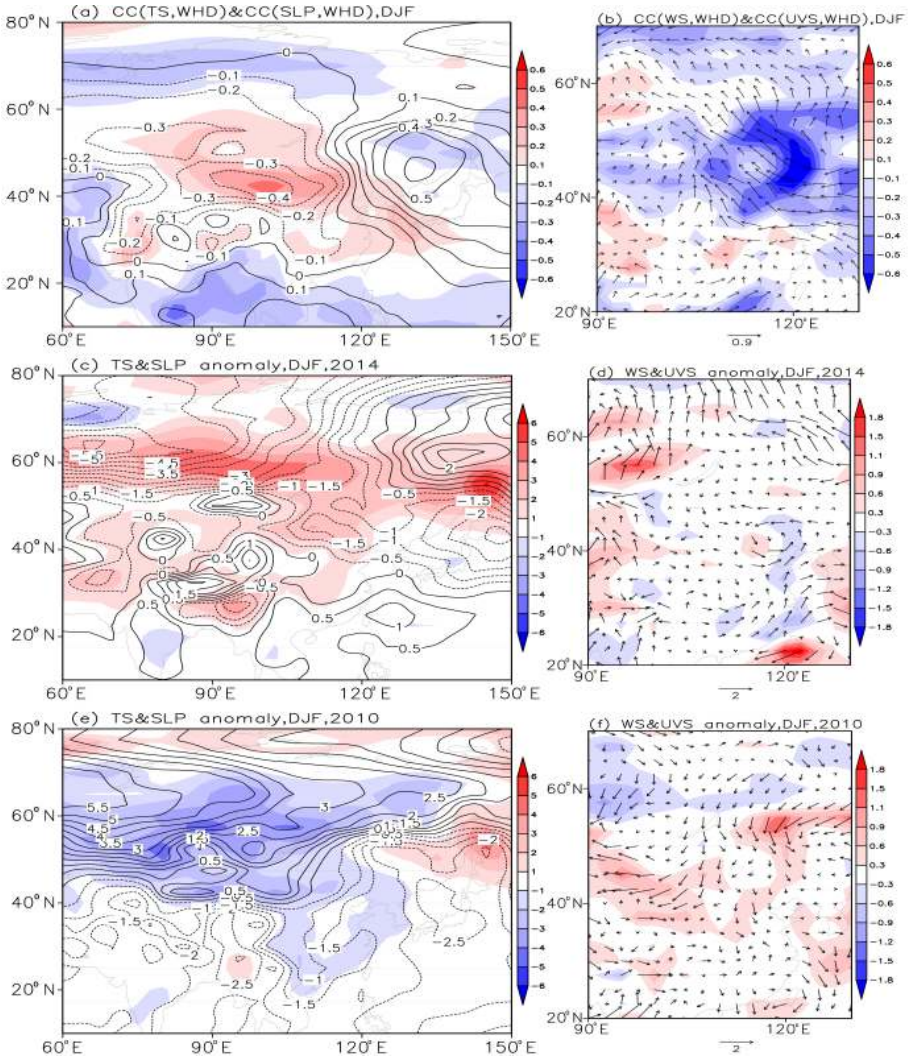

Figure 5. Correlation coefficients between WHD_{NCP} and winter circulations from 1979 to 2012 with the linear trend removed **(a, b)**, as well as circulation anomalies in 2014 **(c, d)** and 2010 **(e, f)**. The circulations in panels **(a, c, e)** are T_S (shade) and SLP (contour), and those in panels **(c, d, f)** are surface wind speed (shade) and wind vector (arrow).

4 Possible mechanisms for the winter haze in 2014

In the above discussion, we addressed the associated circulations that were characterized by EA/WR, WP, and EU patterns and that contributed to the extreme haze pollution in 2014. H. J. Wang et al. (2015) found that the pre-autumn ASI could significantly impact the WHDs in the east of China. As another efficient external forcing, the negative SWP SST anomalies (SSTA) markedly intensified WHD_{NCP} (Yin and Wang, 2016a). Thus, the question arises as to whether these factors could have caused the extreme haze pollution in 2014.

From 1979 onward, the pre-autumn ASI declined substantially, which might impact the winter climate of East Asia (Liu et al., 2012). Furthermore, this decreasing trend of the ASI intensified since 2006 (H. J. Wang et al., 2015). The relationship between the pre-autumn ASI and the circulations was analyzed using the SVD method, explaining 51.6 and 17.9 % of the variance by the first (SVD1) and second (SVD2) mode, respectively. The correlation coefficient of the first temporal series was 0.76, which was significantly above the 99 % confidence level. The excited anticyclonic (A) or cyclonic (C) activity centers of $H500$ in winter were located over the North Atlantic and Europe, to the north of the Caspian Sea, and around Mongolia and North China, which appeared as the positive phase of the EA/WR pattern (Fig. 7a). The corresponding pre-autumn ASI, with more sea ice (SI) over the Barents Sea, Kara Sea, and Laptev Sea (BKLSI) and less SI in the East Siberian Sea (ESSI) could have contributed to the positive EA/WR pattern (Fig. 7b). The anomalous ASI of the eastern Hemisphere in 2014 was similar to that shown in Fig. 7b. According to the SVD results, the pre-autumn ASI anomalies in 2014 might have trig-

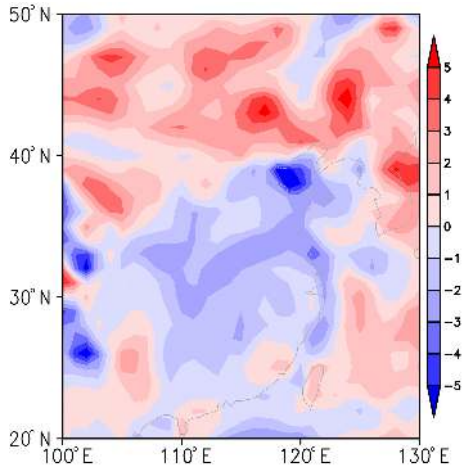

Figure 6. The difference of averaged wintertime PBLH between 2014 and 2010.

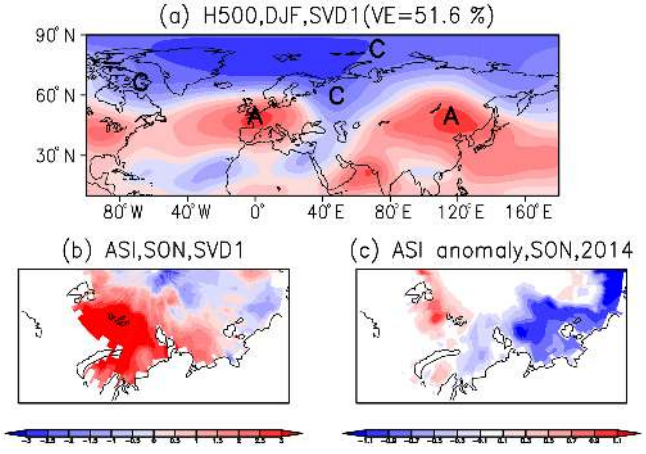

Figure 7. Heterogeneous correlation map of the first SVD mode for detrended and normalized **(a)** $H500$ during DJF and **(b)** ASI during SON 1979–2014, as well as **(c)** the ASI anomalies during SON 2014. Letters A and C in panel **(a)** represent anticyclone and cyclone, respectively.

gered the EA/WR pattern in the atmosphere, especially the anomalous high over the NCP, and led to greater WHD_{NCP}. In autumn 2010, less BKLSI and more ESSI (Fig. S2) occurred, which might have induced fewer WHDs over the NCP.

In winter 2014, the T_s anomalies of the broad region of Eurasia (40–70° N) were clearly positive. EA/WR is a famous continental teleconnection, and a significant land–air interaction could influence the EA/WR pattern. To illustrate this concept, an SVD analysis was performed between the detrended and normalized winter T_s and $H500$ (Fig. 8). The explained variance and correlation coefficient of the first component were 53.3 % and 0.73, respectively. The spatial coefficients of T_s were distributed similarly to T_s anomalies in 2014. The associated circulations displayed three anoma-

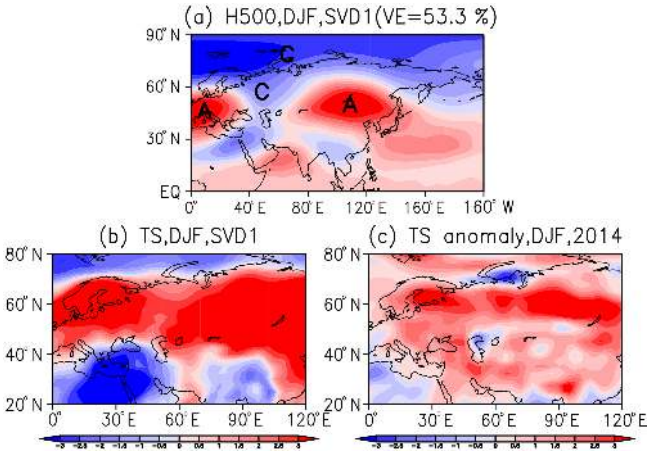

Figure 8. Heterogeneous correlation map of the first SVD mode for detrended and normalized **(a)** $H500$ during DJF and **(b)** T_s during DJF 1979–2014, as well as **(c)** the T_s anomalies during DJF 2014. Letters A and C in panel **(a)** represent anticyclone and cyclone, respectively.

lous centers, i.e., a positive center over Europe, negative anomalies to the north of the Caspian Sea, and another positive center over Mongolia and North China, which were also the three atmospherically active centers of EA/WR on the continent that occurred in winter 2014 (Fig. 5c). These results indicated that the T_s anomalies of winter 2014 could have induced or intensified the positive EA/WR phase and resulted in the extreme WHD_{NCP} case in 2014. In winter 2010, the cooler land surface of midlatitude Eurasia (Fig. S3) could have contributed to the negative EA/WR phase. The diagnostic analyses of two inversely extreme WHD_{NCP} cases enhanced the relationship between the winter midlatitude Eurasia T_s and WHD_{NCP}.

Figures 7 and 8 also show negative anomalies over the polar area (70–80° N, 60–90° E) and a positive center over Mongolia and North China (45–55° N, 90–110° E), which can be recognized as the positive EU phase. When BKLSI was above normal and ESSI was below normal or the surface of midlatitude Eurasia was warmer, these two centers could be stimulated or enhanced, representing favorable circulations for haze occurrence. Prior to this study, Yin and Wang (2016a) found that the pre-autumn SSTA of the Pacific excited the anticyclone anomalies over North China and resulted in more WHD_{NCP}. The SST in October and November (ON) and winter $H500$ were decomposed using the SVD technique to reveal the main relationships. The explained variance and the correlation coefficient of the first component were 60.2 % and 0.73, respectively. An EU-like pattern occurred in the first mode of $H500$, i.e., cyclonic anomalies over the polar area and anticyclonic anomalies over Mongolia and North China (Fig. 9a). The associated SST was cooler over the northwestern Pacific, involving Kuroshio and its extension, and warmer over the central-east Pacific and the Gulf

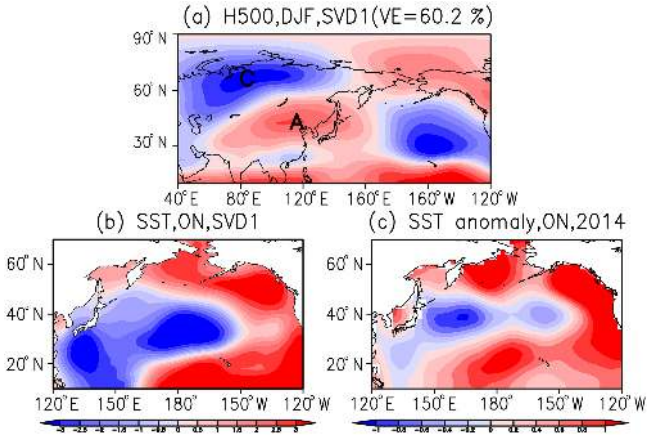

Figure 9. Heterogeneous correlation map of the first SVD mode for detrended and normalized **(a)** $H500$ during DJF and **(b)** SST during ON 1979–2014, as well as **(c)** the SST anomalies during ON 2014. Letters A and C in panel **(a)** represent anticyclone and cyclone, respectively.

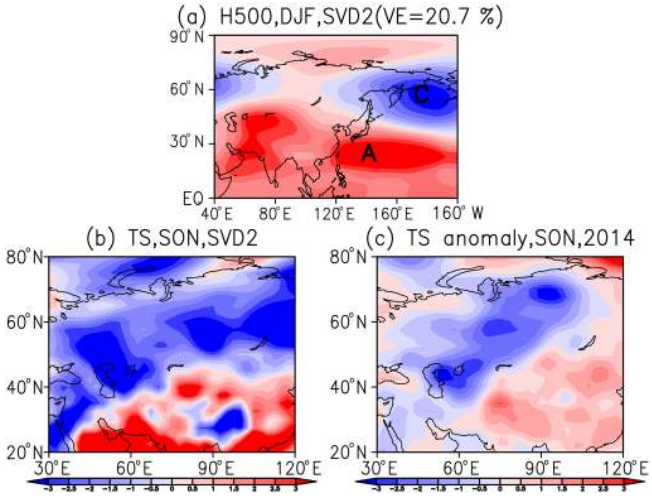

Figure 10. Heterogeneous correlation map of the second SVD mode for detrended and normalized **(a)** $H500$ during DJF and **(b)** T_s during SON 1979–2014, as well as **(c)** the T_s anomalies during SON 2014. Letters A and C in panel **(a)** represent anticyclone and cyclone, respectively.

of Alaska (Fig. 9b). Another atmospheric response was the weaker East Asia trough, indicating weaker EAWM and cold air. Figure 9c shows the ON SSTA of the Pacific in 2014, which appeared to be similar to the SST SVD1 distribution and stimulated haze-prone responses. In 2010, the ON SSTA in the Pacific did not show a well-organized opposite pattern (Fig. S4), but a cooler SST was observed on the central-east Pacific and the Gulf of Alaska, which were of benefit to haze occurrence.

Both EA/WR and EU were continental teleconnection patterns that propagated over Eurasia. In contrast, the WP pattern was located over the junction of the marine and mainland areas, and its positive phases were composed of a broad positive center over the northwestern Pacific and Southeast Asia and a negative center over the Kamchatka Peninsula (Barnston and Livezey, 1987). From Table 1, the stronger WP positive phase could have contributed to more WHD_{NCP} and could also have been partially responsible for the severe haze event in 2014. To identify the causes of such circulations, we performed an SVD analysis between winter $H500$ and pre-autumn T_s, with explained variance of 39.8 and 20.7 %, respectively, for SVD1 and SVD2. The results of SVD2 showed significant anomalies in the two centers of the positive WP pattern and anomalous T_s distributed from the southwest to the northeast in Eurasia (Fig. 10). The correlation coefficient of the SVD2 time series was 0.62, exceeding the 99 % confidence level. Similar to the SVD2 representation, two "southwest to northeast" anomalous T_s distributions also occurred in autumn 2014, i.e., negative anomalies from the Caspian Sea to Lake Baikal and a positive anomalous belt from Southwest China to Northeast China (Fig. 10c). Referring to SVD2, these "southwest to northeast" T_s anomalies could have induced atmospheric responses over the junction of the Pacific and Asian land, which resembled the WP pattern and impacted the local circulations over the NCP area. In autumn 2010, the positive belt of T_s from the Caspian Sea to Lake Baikal was significant, and the land surface of the Tibet Plateau was warmer than normal (Fig. S5). These two anomalies were dramatically opposite compared to the SVD2 results and could have stimulated a negative WP pattern. As argued by two opposite cases, the mechanisms for how the EA/WR and WP patterns and associated external factors impacted the WHD_{NCP} were confirmed.

5 Conclusions and discussions

Except for a few sites, haze pollution over the NCP in winter 2014 was the severest in the past 30 years. In the BSH area and the northeast of Hebei, the number of WHDs increased significantly and moved into the rural area, illustrating a joint and broad severe haze-prone region. The $PM_{2.5}$ concentrations at a GAW station and an urban site were almost equal in winter 2010 and 2014, so there was no evidence that the emissions were more in 2014 than 2010. The climate anomalies played key roles in the formation of heavy haze pollution case in 2014. In the lower and middle troposphere, the positive phases of EA/WR, WP, and EU patterns modulated the local anticyclone anomalies over North China. The anticyclone anomalies over East Asia not only resulted in stable atmospheric stratification and a thinner boundary layer but also led to a southeasterly anomaly that weakened the cold air but enhanced the moisture transport. The atmospheric matter accumulated easily both in the vertical and horizontal direction. In winter 2014, the teleconnection patterns, such as

EA/WR, EU and WP, combined to alter the local climate conditions to contribute to the extreme haze case. SVD analyses indicated that the pre-autumn ASI anomalies of the eastern Hemisphere and the warmer winter surface of Eurasia could have induced or intensified the responses in the atmosphere, resembling a positive EA/WR pattern. These two external forcings, together with the SSTA in the Pacific (i.e., cooler in the northwestern Pacific and warmer in the central-east Pacific and the Gulf of Alaska) might stimulate or enhance positive EU-like patterns. In autumn 2014, the "southwest to northeast" anomalous T_s belts were other factors that efficiently intensified the haze pollution events, which resulted in a positive phase of the WP pattern. The case of 2010, with the least WHD_{NCP}, was diagnosed as an opposite case, which further supports the speculation that the anomalous EA/WR and WR patterns and associated external forcings have a significant impact on WHD_{NCP}. Additionally, as pointed out by H. J. Wang et al. (2015), the Asian high temperature and drought from summer in 2014 was an extreme climate event. Our studies proved that this previous extreme climate event possibly contributed to the serious haze event in the following winter.

The rapid increase in WHD_{NCP} began in January 2013, and in winter 2013 and 2014, WHD_{NCP} was significantly greater than before. The number of WHD_{NCP} in 2013 and 2014 was greater than 50 and almost equal other in the 2 years (Fig. 2). Therefore, the causes of serious haze in 2013 should also be discussed. The EA/WR pattern was well organized and showed a positive phase that was distributed slightly eastwards (Fig. S6). Influenced by the upper EA/WR pattern, the surface wind speed was slower and the PBLH was lower, showing that the horizontal and vertical dispersion of the atmosphere was weaker (Fig. S7). The EU and WP patterns were unclear. The source region of EU even showed characteristics of a negative phase. According to the 2010 and 2014 case studies, the proceeding and simultaneous external forcings could have impacted the WHD_{NCP}. In contrast, the pre-autumn ASI and T_s and winter T_s in 2013 did not show features similar to those in 2014 (Fig. S8). The pre-autumn Pacific SSTA, which was slightly negative in the northwestern Pacific and positive in the Gulf of Alaska and central-east Pacific, could have stimulated positive anomalies over the NCP and weakened the East Asia trough. Thus, it can be observed that, among many external reasons for the extreme haze in 2014, only the pre-autumn Pacific SSTA was distributed similarly in 2013. The EA/WR Rossby wave train was the prominent circulation contributing to WHD_{NCP} in 2013, with a source located over the central North Atlantic. We speculate that the air–sea interaction over North Atlantic excited the EA/WR pattern in the atmosphere and influenced WHD_{NCP} remotely. The correlation coefficients between the EA/WR index and the pre-autumn SST in Atlantic were calculated and were significantly positive to the south of Greenland (Fig. S9b). When the SSTA to the south of Greenland was positive, the responses similar to EA/WR occurred in the atmosphere. The pre-autumn SSTA in the Atlantic in 2013 was similar to that shown in Fig. S9b and might have remotely impacted WHD_{NCP} via the EA/WR pattern. It should be noted that the SSTA of the key region in the Atlantic was negative and had an adverse effect on WHD_{NCP} in 2014.

From the point of facilitating a larger amount of WHD_{NCP}, the associated circulations and external forcings in 2013 were different from that in 2014, but the serious situations of haze were almost the same. In our study, we assumed that energy consumption has increased linearly in the recent years. In such a hypothesis, human activities mainly impacted the long-term trend of WHD_{NCP}. After removal of the linear trend, the interannual variability in haze pollution should be mainly the result of climatic anomalies. The Shangdianzi site is the only GAW station in North China and was chosen to reflect the natural or background situation of the atmosphere. The mean mass concentrations of $PM_{2.5}$ in winter from 2004 to 2014 are plotted in Fig. 11. The concentration in winter 2013 increased abruptly up to nearly twice that in 2010 and 2014 and was the highest in observational history, which is not in agreement with our assumption. Furthermore, the $PM_{2.5}$ concentration of an urban site, Baolian station,

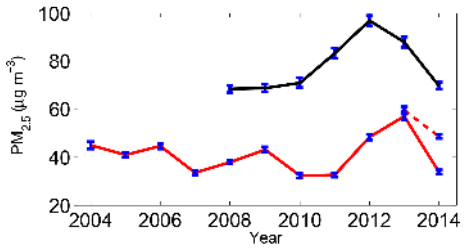

Figure 11. Mean of $PM_{2.5}$ concentration in winter at Shangdianzi Station from 2004 to 2014 as measured by the TEOM (solid) and β-ray (dash) method, and at Baolian Station from 2008 to 2014. The error bar represents 1 standard error among the different measured hours.

Table 2. Summary of the various influence factors for WHD_{NCP}. The "+++" indicates "more important", "++" indicates "important", "+" indicates "less important" , and blank indicates "not important".

Factors	2010	2013	2014
$PM_{2.5}$ concentration	++	+++	++
Local surface wind speed	++	++	++
Local PBLH	++	++	++
EA/WR	++	++	++
WP	++		++
EU			++
Pre-autumn ASI	++		++
Winter T_s	++		++
ON Pacific SSTA	+	++	++
Pre-autumn T_s	++		++
SON Atlantic SSTA		++	

was also much higher than 2010 and 2014. Even though the anomalous circulations were not beneficial enough for haze occurrence, the joint effect of the highest level of pollution emissions and climate conditions could result in a serious haze event. Documented by these three case studies, the influences of the highest $PM_{2.5}$ were the fundamental cause, and the associated atmospheric anomalies and external forcings played key roles in the severe haze pollution. In the case studies, 2010 and 2014 exhibited approximately equal $PM_{2.5}$ concentrations of the background atmosphere, but the associated circulations and external forcings were slightly different. It is possible that not all of the above factors might be found in a specific case study – i.e., a few of these factors played essential roles and led to the characteristics of that case (see a brief summary of the impacts of these factors on WHD_{NCP} in Table 2). In this study, we focused on the roles of climate anomalies, and the impact of human activities will be studied in our future work. Separation of the contributions quantitatively by means of numerical models or advanced statistical approaches would be a meaningful task that would be helpful in the interpretation of the mechanisms and seasonal prediction (Yin and Wang, 2016b).

6 Data availability

Atmospheric data are available from the NCEP/NCAR data archive: http://www.esrl.noaa.gov/psd/data/gridded/data.ncep.reanalysis.html (NCEP/NCAR, 2017). SST data are downloaded from http://www.esrl.noaa.gov/psd/data/gridded/data.noaa.ersst.v4.html (NOAA, 2017). ASI concentration data can be downloaded from the Hadley Centre: http://www.metoffice.gov.uk/hadobs/hadisst/ (HadISST, 2017). The monthly EA/WR and WP indices (CPC, 2017) can be downloaded from NOAA's Climate Prediction Center: http://www.cpc.ncep.noaa.gov/data/teledoc/telecontents.shtml. The ground observations are from the website http://data.cma.cn/ (CMA, 2017). The monthly PBLH data are available on the ERA-Interim website: http://www.ecmwf.int/en/research/climate-reanalysis/era-interim (ERA-Interim, 2017). The atmospheric compositions data can be obtained from the authors.

The Supplement related to this article is available online at doi:10.5194/acp-17-1641-2017-supplement.

Acknowledgements. This research was supported by the National Natural Science Foundation of China (grants 41421004 and 41210007) and CAS-PKU Partnership Program.

Edited by: A. Ding
Reviewed by: two anonymous referees

References

Barnston, A. G. and Livezey, R. E.: Classification, seasonality and persistence of low frequency atmospheric circulation patterns, Mon. Weather Rev., 115, 1083–1126, 1987.

Chen, H. P. and Wang, H. J.: Haze days in North China and the associated atmospheric circulations based on daily visibility data from 1960 to 2012, J. Geophys. Res.-Atmos., 120, 5895–5909, doi:10.1002/2015JD023225, 2015.

Chen, Y., Ebenstein, A., Greenstone, M., and Li, H.: Evidence on the impact of sustained exposure to air pollution on life expectancy from China's Huai River policy, P. Natl. Acad. Sci. USA, 110, 12936–12941, 2013.

China Meteorology Administration: The notification on the adjustment of haze phenomenon observing provisions and revision of fog-haze observation data in 2013 by Observing and Forecasting Department Division, China Meteorology Administration, 2014.

CMA: China ground observation data sets, available at: http://data.cma.cn/, last access: 21 January 2017 (in Chinese).

CPC: CPC Monthly EA/WR and WP Index, available at: http://www.cpc.ncep.noaa.gov/data/teledoc/telecontents.shtml, last access: 21 January 2017.

Cressman, G.: An operational objective analysis system, Mon. Weather Rev., 87, 367–374, 1959.

Dee, D. P., Uppala, S. M., Simmons, A. J., Berrisford, P., Poli, P., Kobayashi, S., Andrae, U., Balmaseda, M. A., Balsamo, G., Bauer, P., Bechtold, P., and Beljaars, A. C. M.: The ERA-Interim reanalysis: configuration and performance of the data assimilation system, Q. J. Roy. Meteor. Soc., 137, 553–597, doi:10.1002/qj.828, 2011.

Ding, Y. H. and Liu, Y. J.: Analysis of long-term variations of fog and haze in China in recent 50 years and their relations with atmospheric humidity, Sci. China Ser. D, 57, 36–46, 2014 (in Chinese).

ERA-Interim: PBLH data sets, available at: http://www.ecmwf.int/en/research/climate-reanalysis/era-interim, last access: 21 January 2017.

HadISST: Hadley Centre Sea Ice and Sea Surface Temperature data sets, available at: http://www.metoffice.gov.uk/hadobs/hadisst/, last access: 21 January 2017.

Kalnay, E., Kanamitsu, M., Kistler, R., Collins, W., Deaven, D., Gandin, L., Iredell, M., Saha, S., White, G., Woollen, J., Zhu, Y., Leetmaa, A., Reynolds, R., Chelliah, M., Ebisuzaki, W., Higgins, W., Janowiak, J., Mo, K. C., Ropelewski, C., Wang, J., Jenne, R., and Joseph, D.: The NCEP/NCAR 40-year reanalysis project, B. Am. Meteorol. Soc., 77, 437–471, doi:10.1175/1520-0477(1996)077<0437:TNYRP>2.0.CO;2, 1996.

Li, Q., Zhang, R. H., and Wang, Y.: Interannual variation of the winter-time fog–haze days across central and eastern China and its relation with East Asian winter monsoon, Int. J. Climatol., 36, 346–354, doi:10.1002/joc.4350, 2015.

Liu, J. P., Curry, J. A., Mirong Song, W. H J., and Horton, R. M.: Impact of declining Arctic sea ice on winter snowfall, P. Natl. Acad. Sci., 109, 4074–4079, doi:10.1073/pnas.1114910109, 2012.

Liu, Y. Y., Wang, L., Zhou, W., and Chen, W.: Three Eurasian teleconnection pattern: spatial structures, temporal variability, and associated climate anomalies, Clim. Dynam., 42, 2817–2839, 2014.

NCEP/NCAR: NCEP/NCAR Reanalysis data sets, available at: http://www.esrl.noaa.gov/psd/data/gridded/data.ncep.reanalysis.html, last access: 21 January 2017.

NOAA: NOAA Extended Reconstructed Sea Surface Temperature (SST) V4 data sets, available at: http://www.esrl.noaa.gov/psd/data/gridded/data.noaa.ersst.v4.html, last access: 21 January 2017.

Rayner, N. A., Parker, D. E., Horton, E. B., Folland, C. K., Alexander, L. V., Rowell, D. P., Kent, E. C., and Kaplan, A.: Global analyses of sea surface temperature, sea ice, and night marine air temperature since the late nineteenth century, J. Geophys. Res., 108, 4407, doi:10.1029/2002JD002670, 2003.

Smith, T., Reynolds, R., Peterson, T., and Lawrimore, J.: Improvements to NOAA's historical merged land–ocean surface temperature analysis (1880–2006), J. Climate, 21, 2283–2296, 2008.

Wallace, J. M. and Gutzler, D. S.: Teleconnection in the geopotential height field during the Northern Hemisphere winter, Mon. Weather Rev., 109, 784–812, doi:10.1175/1520-0493(1981)109<0784:TITGHF>2.0.CO;2, 1981.

Wang, D. Q., Cui, T., Si, D., Shao, X., Li, Q. Q., and Sun, C. H.: Features and Possible Causes for East Asian Winter Monsoon in 2014/2015, Meteorological Monthly, 41, 907–914, 2015 (in Chinese).

Wang, H.-J. and Chen, H.-P.: Understanding the recent trend of haze pollution in eastern China: roles of climate change, Atmos. Chem. Phys., 16, 4205–4211, doi:10.5194/acp-16-4205-2016, 2016.

Wang, H. J. and He, S. P.: The North China/Northeastern Asia Severe Summer Drought in 2014, J. Climate, 28, 6667–668, 2015.

Wang, H. J., Chen, H. P., and Liu, J. P.: Arctic sea ice decline intensified haze pollution in eastern China, Atmos. Ocean. Sci. Lett., 8, 1–9, 2015.

Wang, Y. S., Yao, L., Liu, Z. R., Ji, D. S., Wang, L. L., and Zhang, J. K.: Formation of haze pollution in Beijing–Tianjin–Hebei region and their control strategies, Bull. Chinese Acad. Sci., 28, 353–363, 2013.

Yang, Y., Liao, H., and Lou, S.: Increase in winter haze over eastern China in recent decades: Roles of variations in meteorological parameters and anthropogenic emissions, J. Geophys. Res.-Atmos., 121, 13050–13065, doi:10.1002/2016JD025136, 2016.

Yao, B., Vollmer, M. K., Zhou, L. X., Henne, S., Reimann, S., Li, P. C., Wenger, A., and Hill, M.: In-situ measurements of atmospheric hydrofluorocarbons (HFCs) and perfluorocarbons (PFCs) at the Shangdianzi regional background station, China, Atmos. Chem. Phys., 12, 10181–10193, doi:10.5194/acp-12-10181-2012, 2012.

Yin, Y., Cheng, J., Duan, Y., Wei, H., Ji, R., Yu, J., and Yu, H.: Correlation analysis between the $PM_{2.5}$, PM_{10} which were taken in the hazy day and the number of outpatient about breathing sections, breathing sections of pediatrics in Shanghai, Huan Jing Ke Xue, 32, 1894–1898, 2011 (in Chinese).

Yin, Z. C. and Wang, H. J.: The relationship between the subtropical Western Pacific SST and haze over North-Central North China Plain, Int. J. Climatol., 36, 3479–3491, doi:10.1002/joc.4570, 2016a.

Yin, Z. and Wang, H.: Seasonal prediction of winter haze days in the north central North China Plain, Atmos. Chem. Phys., 16, 14843–14852, doi:10.5194/acp-16-14843-2016, 2016b.

Yin, Z. C., Wang, H. J., and Guo, W. L.: Climatic change features of fog and haze in winter over North China and Huang-Huai Area, Science China Earth Sciences, 58, 1370–1376, 2015a.

Yin, Z. C., Wang, H. J., and Yuan, D. M.: Interdecadal increase of haze in winter over North China and the Huang-huai area and the weakening of the East Asia winter monsoon, Chin. Sci. Bull., 60, 1395–1400, 2015b (in Chinese).

Zhang, R. H., Li, Q., and Zhang, R. N.: Meteorological conditions for the persistent severe fog and haze event over eastern China in January 2013, Science China: Earth Sciences, 57, 26–35, doi:10.1360/972013-150, 2014.

Zhang, Y., Ding, A., Mao, H., Nie, W., Zhou, D., Liu, L., Huang, X., and Fu, C.: Impact of synoptic weather patterns and interdecadal climate variability on air quality in the North China Plain during 1980–2013, Atmos. Environ., 124, 119–128, 2016.

Zhao, N., Yin, Z. C., and Wu, F.: Characteristics of persistent fog and haze process and its forming reason in Beijing, J. Meteorol. Environ., 30, 15–20, 2014 (in Chinese).

Zhao, P. S., Zhang, X. L., Xu, X. F., and Zhao, X. J.: Long-term visibility trends and characteristics in the region of Beijing, Tianjin, and Hebei, China, Atmos. Res., 101, 711–718, 2011.